PHYSICAL REVIEW E **66**, 036403 (2002)

# Simple model for laser-produced, mass-limited water-droplet plasmas

Kurt Garloff,* Michiel van den Donker, and Joost van der Mullen†
*Eindhoven University of Technology, Department of Applied Physics, Equilibrium and Transport in Plasmas, P.O. Box 513,*
*5600 MB Eindhoven, The Netherlands*

Fred van Goor
*Twente University, P.O. Box 217, 7500 AE Enschede, The Netherlands*

Ralph Brummans and Jeroen Jonkers
*Philips Research Laboratories Eindhoven, Professor Holstlaan 4 (WA03), 5656 AA Eindhoven, The Netherlands*

(Received 13 February 2002; published 18 September 2002)

Plasmas, produced by a neodymium yttrium aluminum garnet (Nd:YAG) laser pulse focused on a small water droplet and used for the generation of extreme ultraviolet light, can be described by a relatively simple model due to the fact that thermodynamic equilibrium can be assumed for the most important phase. Only three time-dependent variables—radius, expansion speed, and internal energy—are needed to describe the physics of the plasma. Nevertheless, it predicts quantities such as the size and the spectrum rather well. It is expected that the theory and the model presented here can also be applied to other laser-produced plasmas.

DOI: 10.1103/PhysRevE.66.036403 PACS number(s): 52.65.Cc

## I. INTRODUCTION

Laser-produced plasmas are promising sources for the generation of extreme ultraviolet (EUV) and soft x rays in important future applications, for instance EUV lithography [1–3], where multilayer mirrors are used to focus radiation of 11.5 or 13.4 nm wavelength, and water window microscopy [2,4], where wavelengths between 2.3 and 4.4 nm are used. A high peak power laser is being used to create a plasma in a gas, a liquid or in solid-state material. In the past solid-state targets were widely used, since high conversions efficiencies from laser light to (soft) x rays can be achieved [5]. Unfortunately, these targets also suffer from relatively high emission of material, leading to contamination of the condenser optics and thus limiting its lifetime [6,7]. The so-called mass-limited targets seem to avoid this problem, which leads to the proposals of using condensed or clustered noble gases by Kubiak *et al.* [8] or liquid droplets by Hertz and co-workers [9]. With these new targets conversion efficiencies up to several percents have been obtained in the water window [10–12] and up to a percent in the EUV region [6,8,13,14].

At Philips Research an EUV source based on water droplets has been operational since the beginning of 1999 [7,15]. The principle of operation of the source is very similar to the droplet-based sources described elsewhere [8,10,16]. In our case a frequency doubled neodymium yttrium aluminum garnet (Nd:YAG) laser with up to 0.45 J in a 10-ns FWHM (full width at half maximum) pulse is being focused on a water droplet with approximately 20 $\mu$m diameter. There is one important constructional difference from other setups: on our setup, a differential pumping scheme is applied for those droplets that are not being used for the EUV production [7,15]. Compared to the more commonly used cryogenic cooling this feature has the advantage that it allows continuous operation. The source has been characterized intensively [15] and recently it has been used successfully for the characterization of EUV optics [17].

A model has been developed to improve the understanding of the processes taking place inside the plasma and to support the experimental efforts to improve the performance of the source. It appears that important approximations can be made as a consequence of the mass-limited nature of such a plasma. This results in a relatively simple and elegant model. But in spite of the simplicity of the model, good agreement with the experimental results has been found.

## II. MODEL

The main assumptions of the model are explained in the following five sections. With these assumptions the plasma can be described using three coupled time-dependent differential equations, see Sec. II F. Section II G deals with the initial conditions.

### A. Homogeneous sphere

The plasma is assumed to be a homogeneous sphere. This may be a crude simplification since the absorption of the laser energy can be a local process. However, due to the high heat conduction of the plasma and the fact that the absorption coefficient is low at the beginning, it is to be expected that thermal gradients in the plasma are small. Treating the plasma as a homogeneous sphere is supported by pinhole pictures [7,15] which show (1) that the plasma has a spherical shape, (2) that the EUV emission is a function of the radial position only, i.e., there is no difference in EUV along or perpendicular to the laser beam, and (3) that the emission from the plasma is isotropic.

---

*Corresponding author. Email address: kurt@garloff.de
†Electronic address: J.J.A.M.v.d.Mullen@TUE.NL

1063-651X/2002/66(3)/036403(13)/$20.00

The fact that good agreement between the modeled and the experimental results is found (see Sec. III) may also support this assumption.

### B. Expansion velocity

As soon as the plasma is created the density and the temperature are high, so that the resulting pressure is of the order of $10^9$ Pa, which is many orders of magnitude higher than that of the surrounding vacuum ($10^{-2}$–$10^1$ Pa). Therefore the plasma starts to explode. During this process thermal energy is converted into directed kinetic energy, similar to an adiabatic expansion. Note that in this case the expansion is not adiabatic, since at the same time the plasma is still heated by the laser.

From the assumption that the plasma is a homogeneous sphere it follows that the directed velocity is proportional to the radial position. It can easily be shown that the total kinetic energy related to the expansion equals

$$E_{\mathrm{exp}}=\int_V \frac{1}{2}\varrho\left(v_{\mathrm{exp}}\frac{r}{R}\right)^2 d^3r=\frac{3}{10}Mv_{\mathrm{exp}}^2, \tag{1}$$

in which $M$ is the total mass of the water droplet, $\varrho$ is the mass density, $R$ and $V$ are the time-dependent radius and the volume of the plasma, respectively, and $v_{\mathrm{exp}}=v(R)$ is the velocity of the plasma-vacuum boundary. The power dissipated in the expansion process $P_{\mathrm{exp}}$ is given by

$$P_{\mathrm{exp}}=p\frac{\partial}{\partial t}V=nk_{\mathrm{B}}T4\pi R^2 v_{\mathrm{exp}}, \tag{2}$$

in which $n$ and $p$ are the total density and pressure of the plasma, respectively. The temperature of the electrons and of the heavy particles is assumed to be equal to the plasma temperature $T$, which is discussed in Sec. II C 1.

Combining these two expressions results in a differential equation for the acceleration of the expansion

$$\frac{\partial}{\partial t}v_{\mathrm{exp}}=5\alpha_{\mathrm{diss}}(1+\alpha_{\mathrm{ion}})\frac{k_{\mathrm{B}}T}{m_{\mathrm{H_2O}}R}, \tag{3}$$

with

$$\alpha_{\mathrm{ion}}=\frac{n_e}{n_{\mathrm{H}}+n_{\mathrm{O}}} \tag{4}$$

being the ionization ratio, $n_e$ the electron number density, and $n_{\mathrm{H}}$ and $n_{\mathrm{O}}$ the sums of the number densities of hydrogen and oxygen atoms and ions, respectively. The dissociation ratio $\alpha_{\mathrm{diss}}$ equals three, since the model starts after the water is completely dissociated and some electrons have been produced by the laser. Note that the mass of a single water molecule $m_{\mathrm{H_2O}}$ appears in this formula. The acceleration of the expansion depends on the ratio of the number of particles, determining the pressure that is the driving force of the expansion, and their total mass, determining the inertia. This equation is valid as long as the pressure in the plasma is much higher than that of the surroundings so that no shock occurs.

### C. Local thermodynamic equilibrium

In this section criteria for the validity of local thermodynamic equilibrium (LTE) are derived.

LTE has two important aspects: (1) thermal equilibrium i.e., the electron temperature $T_e$ equals that of the heavy particles $T_h$ so that the plasma can be described by one temperature $T$ and (2) Saha-Boltzmann equilibrium, i.e., the relative densities of the excited states and the various ionization stages are given by Saha-Boltzmann relations.

The derived criteria depend on plasma quantities such as the electron density and temperature, which are time-dependent quantities. These can only be verified for the initial conditions; the validity of LTE when the plasma evolves is verified in Sec. III B, where these quantities are presented as results of the model. It is found that the plasma can considered to be in LTE for at least the most important first part of the time evolution when the laser power is coupled in and the EUV radiation is produced.

#### *1. Thermal equilibrium*

In thermal equilibrium the electron energy distribution function can be correctly described by a Maxwellian distribution with one-electron temperature $T_e$; similarly the heavy particles can be assigned a temperature $T_h$ that equals $T_e$.

Many laboratory plasmas are not in thermal equilibrium, since the heat transfer of the electrons to the heavy particles is not very efficient (due to the large mass ratio) whereas the heavy particles can lose their energy towards the surroundings relatively efficiently. However, at high electron densities the low energy transfer in one-electron–heavy-particle collision is compensated by the large frequency of those collisions, so that thermal equilibrium may be established. To see whether thermal equilibrium holds in our case, we take a look at the heat balance of the heavy particles (with the number density $n_h$), which can be approximately written in the following form:

$$n_h\frac{3}{2}k_{\mathrm{B}}\frac{d}{dt}T_h=\nu_{eh}^{T_h}n_h\frac{3}{2}k_{\mathrm{B}}(T_e-T_h)-\nu_{\mathrm{exp}}^{T_h}n_h\frac{3}{2}k_{\mathrm{B}}T_h, \tag{5}$$

i.e., the change in the heavy-particle thermal energy equals the net heating by elastic collisions with the free electrons and the cooling by the expansion, the first and the last term at the right hand side, respectively. Note that the energy changes due to radiation and power incoupling is not included in this equation, as it does not affect the kinetic energy of the heavy particles directly.

Introducing the transient frequency for the heating of the heavy particles,

$$\nu_{\mathrm{tr}}^{T_h}\equiv\frac{1}{k_{\mathrm{B}}T_h}\frac{dk_{\mathrm{B}}T_h}{dt}, \tag{6}$$

Eq. (5) can also be written as

$$T_e \nu_{eh}^{T_h} = T_h (\nu_{eh}^{T_h} + \nu_{\mathrm{exp}}^{T_h} + \nu_{\mathrm{tr}}^{T_h}) \tag{7}$$

or as an expression for the deviation from thermal equilibrium:

$$T_e = T_h \left( 1 + \frac{\nu_{\mathrm{exp}}^{T_h}}{\nu_{eh}^{T_h}} + \frac{\nu_{\mathrm{tr}}^{T_h}}{\nu_{eh}^{T_h}} \right). \tag{8}$$

This last equation (8) states that thermal equilibrium holds when the cooling frequencies of the heavy particles due to the expansion and the transient frequency are much smaller than the kinetic energy transfer from the heavy particles to the electrons. This is generalized in the concept of "disturbed bilateral relations" [18], which states that equilibrium holds when the equilibrium disturbing frequencies are much smaller that the equilibrium restoring frequencies.

As is shown in the preceding section, the cooling of the heavy particles due to the expansion of the plasma is given by

$$P_{\mathrm{exp}}^{h} = p_h \frac{\partial}{\partial t} V = n_h k_{\mathrm{B}} T_h 4 \pi R^2 v_{\mathrm{exp}}. \tag{9}$$

The total thermal energy of the heavy particles equals

$$E_{\mathrm{th}}^{h} = n_h V \frac{3}{2} k_{\mathrm{B}} T_h = n_h k_{\mathrm{B}} T_h 2 \pi R^3, \tag{10}$$

so that the cooling frequency of the heavy particles due to the expansion becomes

$$\nu_{\mathrm{exp}}^{T_h} \equiv \frac{P_{\mathrm{exp}}^{h}}{E_{\mathrm{th}}^{h}} = \frac{2 v_{\mathrm{exp}}}{R}. \tag{11}$$

The frequency for kinetic energy exchange between the electrons and the heavy particles (and vice versa) equals

$$\nu_{eh}^{T_h} = \sum_i \frac{2 m_e}{m_i} \nu_{ei} = \sum_i \frac{2 m_e}{m_i} n_i \langle \sigma_{ei}^{m} v_e \rangle, \tag{12}$$

where $\nu_{ei}$ is the collision frequency for momentum exchange. The cross section for momentum transfer averaged over the Maxwellian energy distribution is given by Mitchner and Kruger [19]:

$$\langle \sigma_{ei}^{m} v_e \rangle \approx \frac{4\sqrt{2\pi}}{3} \left( \frac{e^2}{4 \pi \epsilon_0 m_e} \right)^2 \left( \frac{m_e}{k_{\mathrm{B}} T_e} \right)^{3/2} Z_i^2 \ln\left( \sqrt{1 + \eta^2 \Lambda_i^2} \right), \tag{13}$$

in which the Coulomb logarithm can be written as

$$\ln\left( \sqrt{1 + \eta^2 \Lambda_i^2} \right) \approx \ln \Lambda_i \quad \text{for} \quad \Lambda_i \gg 1, \tag{14}$$

$$\Lambda_i = \frac{3 k_{\mathrm{B}} T_e 4 \pi \epsilon_0}{Z_i e^2} \sqrt{\frac{\epsilon_0 k_{\mathrm{B}} T_e}{e^2 n_e}}, \tag{15}$$

and $\eta$ being a factor close to unity.

The transient frequency cannot be expressed in plasma quantities only, as the change rate of the heavy-particle temperature $T_h$ is not known in advance. Actual comparison of the different frequencies (and thus the validation of thermal equilibrium) is therefore made in Sec. III B, where the results of the model are presented.

#### *2. Saha-Boltzmann equilibrium*

In case the Saha balance of ionization and recombination

$$X_p^{(Z-1)+} + e \overset{\text{Saha}}{\leftrightarrow} X^{Z+} + e + e \tag{16}$$

is in equilibrium, the relative densities of two subsequent ionization stages are given by the Saha equation. Combining it with the Boltzmann distribution of the atomic state densities yields

$$\frac{n(Z-1,p)}{g(Z-1,p)} = \frac{n_e}{2} \frac{n(Z)}{Q(Z)} \left( \frac{h}{\sqrt{2 \pi m_e k_{\mathrm{B}} T}} \right)^3 \exp\left( \frac{I(Z-1,p)}{k_{\mathrm{B}} T} \right), \tag{17}$$

in which the partition function $Q(Z)$ is defined as

$$Q(Z) \equiv \sum_{p \in \text{all levels}} g(Z,p) \exp\left( -\frac{E(Z,p)}{k_{\mathrm{B}} T} \right). \tag{18}$$

Here $g(Z,p)$ and $E(Z,p)$ represent the statistical weight and the excitation energy of level $p$, respectively, and $I(Z-1,p)$ denotes the ionization energy needed to remove the electron at level $p$ from its atom or ion with charge $Z-1$.

Note that the partition sum as given by Eq. (18) is not well defined since there are in principle infinite excited states with a finite excitation energy. However, the highly excited states are only weakly bound to the ion. In a plasma these states may not be bound at all due to the microelectric fields due to charge fluctuations within the Debye sphere. This effect leads to a lowering of the ionization energy as given by [20],

$$\Delta I_Z = (Z+1) \frac{e^2}{4 \pi \epsilon_0 \lambda_{\mathrm{Debye}}} \tag{19}$$

with the Debye length being defined as

$$\lambda_{\mathrm{Debye}} = \sqrt{\frac{\epsilon_0 k_{\mathrm{B}} T}{e^2 n_e}}. \tag{20}$$

In many low pressure plasmas the Saha balance is disturbed by the outward diffusion of charged particles. In our case deviations from Saha may occur due to the expansion of the plasma and/or transient effects. Using the concept of "disturbed bilateral relations" [18], it can be easily shown that Saha equilibrium between ionization stage $Z-1$ and $Z$ holds when

$$|\nu_{\mathrm{exp}}^{+}(Z) + \nu_{\mathrm{tr}}^{+}(Z)| \ll \nu_{\mathrm{rec}}^{+}(Z), \tag{21}$$

in which the transient frequency is defined as

$$\nu_{\mathrm{tr}}^{+}(Z) \equiv \frac{1}{n(Z)} \frac{dn(Z)}{dt}. \tag{22}$$

For the three particle recombination frequency the Thomson approximation [21] is used,

$$\nu_{\mathrm{rec}}^{+}(Z) = 2.6\times 10^{-39} \frac{Z^3}{\hat{T}^{4.5}} n_e^2, \tag{23}$$

in which the plasma temperature $\hat{T}$ is expressed in eV and $n_e$ in $m^{-3}$, yielding $\nu_{\mathrm{rec}}^{+}(Z)$ in $\mathrm{s}^{-1}$. Due to the expansion of the plasma the density of all species drops, so that the Saha balance (16) shifts to the right. The density of every ionization stage drops, but the ratio of two subsequent ionization stages and thus Saha equilibrium is only affected by the decrease of electron density. Therefore the disturbance frequency due to expansion is given by

$$\nu_{\mathrm{exp}}^{+}(Z) = \frac{1}{n(Z)} \frac{\partial n(Z)}{\partial t}\bigg|_{\mathrm{exp}} = \frac{1}{n(Z)} \frac{\partial n(Z)}{\partial n_e} \frac{\partial n_e}{\partial t}\bigg|_{\mathrm{exp}}. \tag{24}$$

From the Saha equation (17) it can be deduced that

$$\frac{1}{n(Z)} \frac{\partial n(Z)}{\partial n_e} = -\frac{1}{n_e} + \left(\frac{3}{2T} + \frac{I(Z-1)}{T^2}\right) \frac{\partial T}{\partial n_e}, \tag{25}$$

in which the last term at the right-hand side may be neglected, due to the weak dependence of the temperature on the electron density. The decay rate of the electron density due to the expansion of the plasma equals

$$\frac{\partial n_e}{\partial t}\bigg|_{\mathrm{exp}} = -\frac{n_e \partial V}{V\, \partial t} = -\frac{3 v_{\mathrm{exp}}}{R} n_e, \tag{26}$$

so that the expansion disturbance frequency becomes

$$\nu_{\mathrm{exp}}^{+}(Z) = \frac{3 v_{\mathrm{exp}}}{R}. \tag{27}$$

Note that although the densities decrease due to the expansion, the sign of the disturbance frequency is positive since a decrease in electron density shifts the Saha balance to the right, so that the density of the higher ionization stages increases.

In Sec. III B the different frequencies are compared.

### D. Absorption of the laser light

The model describes the development of the plasma in time after the first free electrons have been created by multiphoton ionization. The relevant physics of this last process is included in the initial conditions of the model, which are discussed in Sec. II G. The amount of laser light which is absorbed depends on three quantities: (1) the absorption coefficient of the laser light, (2) the reflection of the laser light on the vacuum-plasma interface, and (3) the spatial overlap between the plasma and the laser focus.

In case the electron density is high enough the inverse *Bremsstrahlung* is the dominant mechanism for absorption of the laser power. The absorption coefficient is given by [22,23]

$$\kappa_{1B} = \frac{\omega_{\mathrm{pl}}^2}{\tilde{n}(\omega_{\mathrm{laser}})c} \frac{\nu_{ei}}{\omega_{\mathrm{laser}}^2 + \nu_{ei}^2}, \tag{28}$$

in which $\omega_{\mathrm{laser}}$ represents the laser angular frequency, $\omega_{\mathrm{pl}}$ the plasma frequency, and $\overline{n}$ the refractive index. The electron-ion collision frequency for *momentum* transfer $\nu_{ei}$ as given in Sec. II C is used, since the quivering speed of the electrons in the laser field is much smaller than the thermal velocity. The refractive index $\tilde{n}$ equals [22]

$$\tilde{n}(\omega) = \frac{1}{\sqrt{2}} \left( (1-\zeta) + \sqrt{(1-\zeta)^2 + \left(\zeta \frac{\nu_{ei}}{\omega}\right)^2} \right)^{1/2}, \tag{29}$$

$$\zeta(\omega) \equiv \frac{\omega_{pl}^2}{\nu_{ei}^2 + \omega^2}. \tag{30}$$

At the interface between vacuum and plasma there is a jump in refractive index and absorption coefficient, so that a part $\rho$ of the light gets reflected. For the sake of simplicity, only perpendicular incidence is assumed, see Eq. (1.21) in Ref. [22] and Eq. (4.83) in Ref. [24],

$$\rho = \frac{[\tilde{n}(\omega_{\mathrm{laser}}) - 1]^2 + \dfrac{(\lambda_{\mathrm{laser}} x_{1\mathrm{B}})^2}{(4\pi)^2}}{[n(\omega_{\mathrm{laser}}) + 1]^2 + \dfrac{(\lambda_{\mathrm{laser}} \kappa_{1\mathrm{B}})^2}{(4\pi)}}. \tag{31}$$

As the reflection is higher for gracing incidence, the assumption of perpendicular incidence results in a slight overestimation of the absorption at the initial phase, when the droplets size is comparable to the laser focus. This is mitigated by the fact that in reality the laser focus is not uniform as assumed below (32), but more resembles a Gaussian shape.

The laser light that manages to cross the boundary between vacuum and plasma gets partially absorbed and partially transmitted. Possible multiple reflections of the laser light are not taken into account. The fraction of absorbed light needs to be corrected for the fact that the plasma may be smaller than the laser focus $R_f$, so the effective fraction of laser light $\chi$ that gets absorbed is

$$\chi = (1-\rho)[1 - \exp(-2\kappa_{1\mathrm{B}} R)] \min\left[\frac{R^2}{R_i^2}, 1\right]. \tag{32}$$

For reasons of simplicity all the laser light is assumed to pass through the center of the plasma, which introduces a small error in the absorption length if the size of the plasma is smaller than or in the same order as the laser focus.

In Fig. 1 the relative absorption is given as a function of the electron density for given plasma radius, ionization ratio, and temperature (assuming $R = R_f$). It can be seen that the relative fraction of the laser power absorbed by the plasma reaches its maximum below the critical electron density $n_e^{\mathrm{crit}}$,

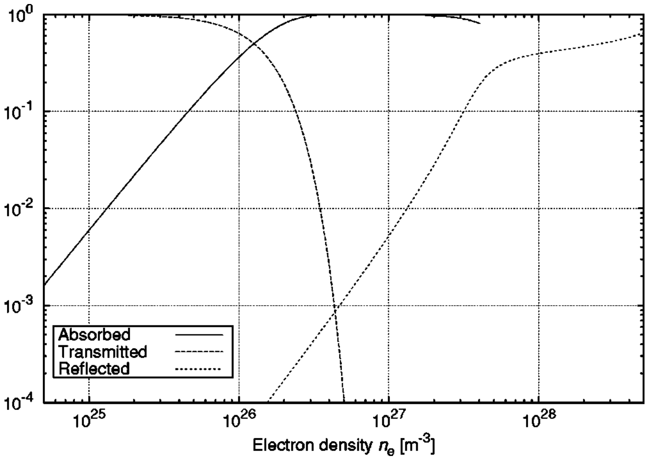

FIG. 1. The absorption, transmission, and reflection of an artificial plasma as functions of the electron density for constant temperature, plasma radius, and ionization ratio of oxygen $\alpha_O$ and hydrogen $\alpha_{\mathrm{H}}$: $T = 15$ eV, $R = 40$ $\mu$m, $\alpha_O = 5$, and $\alpha_{\mathrm{H}} = 1$, respectively. [See Eq. (46) for the definition of the ionization ratios.] Most of these combinations of plasma quantities may not be realized in reality, but this graph is purely for illustrating the dependence of the absorption on the electron density.

i.e., the electron density at which the plasma frequency equals the frequency of the laser light,

$$n_e^{\mathrm{crit}} = \frac{m_e \epsilon_0 \omega_{\mathrm{laser}}^2}{e^2} \approx 4 \times 10^{27} \ \mathrm{m}^{-3}. \tag{33}$$

For electron densities closer to the critical density the step in the absorption coefficient at the vacuum-plasma interface becomes too large and most of the laser power is reflected, as seen from Fig. 1. This effect slows down the increase in the electron density $n_e$, as the heating by the laser becomes less efficient again, once a certain $n_e$ has been reached. This effectively leads to a stabilization of the plasma parameters below the critical density.

### E. Radiation

For most plasmas it is difficult to model (a part of) the spectrum since besides emission absorption also has to be taken into account. For the present case this is largely simplified since it is assumed that the plasma is a homogeneous sphere in thermal equilibrium, so that the local emission and absorption coefficient are constant throughout the plasma. This means that the spectrum can be divided into three different regions, depending on the optical depth $\tau(\lambda)$, which is the product of absorption coefficient $\kappa(\lambda)$ and the plasma radius $R$: (1) optically thick, $\tau(\lambda) \gg 1$, in these parts of the spectrum the plasma acts as a surface radiator with the black body intensity distribution, (2) optically thin, $\tau(\lambda) \ll 1$, so that no absorption has to be taken into account at all, and (3) intermediate optical thickness, $\tau(\lambda)$ in the order of unity, so that absorption has to be explicitly dealt with in the model.

Roughly, it can be stated that visible and longer wavelengths are optically thick and the EUV region is optically thin. These parts of the spectrum can thus be easily calculated. In the UV region in between the optical depth is in the order of unity and the observed emission may be calculated integrating the local emission of the plasma multiplied by its effective escape over the plasma volume. For nonhomogeneous parameters, radiation transport methods, such as ray-tracing or Monte Carlo methods would need to be used.

However, for reasons of simplicity it is assumed that the spectrum at a given wavelength is either optically thick or thin. The wavelength $\lambda_{\mathrm{thick}}$ above which the plasma is optically thick is obtained from comparing the intensity of the continuum emission to that of a black body (Planck limit),

$$I_{\mathrm{BB}}(\lambda, T) = \frac{8\pi h c^2}{\lambda^5 \left[ \exp\left( \frac{hc}{\lambda k_{\mathrm{B}} T} \right) - 1 \right]} \tag{34}$$

with the same temperature $T$:

$$\frac{4\pi}{3} R^3 j_{\mathrm{cont}}(\lambda_{\mathrm{thick}}, T, n_e) = 4\pi R^2 I_{\mathrm{BB}}(\lambda_{\mathrm{thick}}, T). \tag{35}$$

The plasma is considered optically open for all radiation below $\lambda_{\mathrm{thick}}$. For the continuum emission the expression for electron-ion *Bremsstrahlung* given by Brussaard and van de Hulst [Ref. [25], Eq. (22)] or by Hughes [Ref. [22], Eq. (2.68)] (multiplied with full solid angle $4\pi$ and two polarizations and the Cillie factor) is used:

$$\begin{aligned} j_{\mathrm{cont}}(\lambda, T, n_e) = {} & \tilde{n} \frac{64\pi}{3} \left( \frac{e^2}{4\pi\epsilon_0} \right)^3 \sqrt{\frac{m_e}{2\pi k_{\mathrm{B}} T}} \frac{n_e}{m_e^2 c^2 \lambda^2} \\ & \times \exp\left( -\frac{hc}{\lambda k_B T} \right) \frac{\pi}{\sqrt{3}} \sum_Z n(Z) Z^2 [G_{\mathrm{ff}}(\lambda, T) \\ & + G_{\mathrm{fb},Z}(\lambda, T)]. \end{aligned} \tag{36}$$

For the Gaunt factor the free-free (*Bremsstrahlung*) radiation holds [22]:

$$\begin{aligned} G_{\mathrm{ff}}(\lambda, T) &= \frac{\sqrt{3}}{\pi} \exp\left( \frac{hc}{2\lambda k_{\mathrm{B}} T} \right) K_0\left( \frac{hc}{2\lambda k_{\mathrm{B}} T} \right) \\ &\approx \begin{cases} \frac{\sqrt{3}}{\pi} \sqrt{\frac{\pi \lambda k_{\mathrm{B}} T}{hc}} & \text{if } k_B T < hc/\lambda, \\ \frac{\sqrt{3}}{\pi} \ln\left( \frac{4\lambda k_{\mathrm{B}} T}{\gamma_g h c} \right) & \text{if } k_{\mathrm{B}} T > hc/\lambda, \end{cases} \end{aligned} \tag{37}$$

with $K_0(x)$ being the modified Bessel function of the second kind (also referred to as Macdonald or Basset function) and $\gamma_g \approx 1.781$ being the exponent of the Euler's constant.

For the free-bound (recombination) radiation, we calculate the effective Gaunt factor $G_{\mathrm{fb}}$ by summing over the levels recombined into

$$G_{\mathrm{fb},Z}(\lambda, T) = \frac{I_{Z-1}}{k_{\mathrm{B}} T} \sum_p p^{-5} g_P \exp\left( \frac{I_{Z-1} - E_p}{k_{\mathrm{B}} T} \right) \tilde{g}_p(\lambda). \tag{38}$$

The sum is carried out over all the excited levels $p$ of the ionization stage $Z-1$. $I_{Z-1}$ denotes the ionization energy from stage $Z-1$ to $Z$, $p$ denotes the principal quantum number of the level, $g_p$ it's degeneracy, and $E_p$ it's energy with respect to the ground state of ion stage $Z-1$. $\tilde{g}_p(\lambda)$ is the Gaunt factor for the transition in question and is calculated by implementing the hypergeometric functions used by Ref. [26], Eq. (1.21) and reproduced in Ref. [25], Fig. 8.

The exponent in the continuum radiation comes from summing over the electron energy distribution function (EEDF) and reflects our assumption of a Maxwellian EEDF. The exponent in the Gaunt factor for free-bound transitions corrects for the fact, that only a part of the energy comes from the free electrons. For the high densities present in the plasma studied here, the collision times between electrons are in the order of $10^{-14}$ s, which justifies the assumption of a Maxwellian EEDF.

The intensity of a spectral line is obtained from

$$J[\lambda(Z,p,q)]=\begin{cases} \dfrac{n(Z)}{Q(Z)}\exp\left(-\dfrac{E(Z,p)}{k_{\mathrm{B}}T}\right)g(Z,p)A(Z,p,q)\,\dfrac{hc}{\lambda(Z,p,q)} & \text{if } \lambda(z,p,q)<\lambda_{\mathrm{thick}}, \\ 0 & \text{if } \lambda(Z,p,q)>\lambda_{\mathrm{thick}}. \end{cases} \tag{39}$$

The transition probabilities $A(Z,p,q)$, the statistical weights $g(Z,p)$ as well as the excitation and ionization energies $E(Z,p)$ have been obtained from the $A_{\mathrm{MODS}}$ [27] and the Kurucz [28] databases and written to text files that are read by the model upon initialization.

Below the $\lambda_{\mathrm{thick}}$ limit, we have lines that could still exceed the Planck limit. Therefore, the line broadening is calculated and lines are cut off to not exceed Planck limit.

The most strong broadening mechanism is electron impact broadening that yields a Lorentz profile with a line width $\Delta\omega$ of [Ref. [29], Eq. (7.5.24)],

$$\Delta\omega\approx\frac{n_e\pi^3C_2^2}{\langle v_e\rangle}\left[0.923-\ln\left(\frac{\pi C_2}{\rho_{\max}\langle v_e\rangle}\right)\right], \tag{40}$$

$$C_2=a_0\frac{Ze^2}{\hbar}. \tag{41}$$

For the cutoff radius $\rho_{\max}$, the Debye length has been chosen, and the average electron velocity $\langle v_e\rangle$ has been evaluated to $\sqrt{2k_{\mathrm{B}}T/m_e}$. The Doppler broadening (see e.g. Refs. [30] or [31]) with its Gaussian profile does turn out to be less strong than electron impact broadening and has thus been neglected.

### F. Equations and solver

Using the assumptions given above the whole plasma is described by three variables: expansion velocity $v_{\exp}$, temperature and heavy particle density. However, because of numerical reasons the combination $v_{\exp}$, plasma radius $R$, and internal energy $U_{\mathrm{int}}$ (which here is defined as the sum of the energies stored by ionization and excitation and the thermal energy $3/2nk_{\mathrm{B}}T$) is taken. The plasma radius gives, together with the initial size of the water droplet, the total densities of oxygen and of hydrogen. The combination of these densities with $U_{\mathrm{int}}$ gives a unique temperature $T$ and electron density $n_e$, which is obtained by solving a set of Saha equations (one for each two subsequent ionization stages) and charge neutrality. Some iterations are needed to find those values: From a given temperature $T$, the densities of the ions $n(Z)$ and electrons $n_e$ can be calculated; however, as the Saha equation (17) needs the electron density $n_e$, the newly counted $n_{e,\mathrm{new}}$ is used to correct the old one (relaxation factor 0.5) and the calculation is repeated until convergence. The calculated self-consistent combination of $T$ and $n_e$ then is used to calculate the total energy $U_{\mathrm{int}}$, and a solver (Newton-Raphson) is used to determine the correct value for $T$.

This quasi-steady-state solution of the plasma temperature and densities is correct, since transient effects are small at the beginning of the plasma evolution, the most interesting phase, where most of the radiation is produced.

The evolution of the plasma is obtained from solving a set of three coupled differential equations:

$$\frac{\partial}{\partial t}R=v_{\exp}, \tag{42}$$

$$\frac{\partial}{\partial t}v_{\exp}=15(1+\alpha)\,\frac{k_BT}{m_{\mathrm{H_2O}}R}, \tag{43}$$

$$\frac{\partial}{\partial t}U_{\mathrm{int}}=\chi P_{\mathrm{laser}}-P_{\exp}-P_{\mathrm{rad}}. \tag{44}$$

The first differential equation is straightforward, the second is discussed in Sec. II B and the third one is just the power balance (first law of thermodynamics) of the plasma. $P_{\exp}$ is given by Eq. (2) and $P_{\mathrm{rad}}$ represents radiation losses, see Sec. II E.

Note that a different choice of variables could be made; e.g., the electron density $n_e$ be used instead of the internal energy $U_{\mathrm{int}}$ and linked to the power balance by introducing a heat capacity. However, care has to be taken to correct for the fact that the electron density lowers due to the expansion as well, which in LTE corresponds to a lower temperature $T$ and thus a lower energy. This effect needs to be accounted for correctly, which would result in a need to introduce a nontrivial definition of the heat capacity for an expanding plasma.

The set of differential equations is solved numerically using the fourth-order Adams-Bashforth-Moulton (ABM) algorithm [32,33]. This predictor-corrector technique has a fixed time step but requires only two evaluations of the partition sums, the Saha relations and the radiation loss calculation per time step compared to four for the more conventional Runge-Kutta algorithm [32]. This appears to be more significant for the total amount of time required for one complete calculation than the advantage of flexible time steps which Runge-Kutta offers. Note that the ABM algorithm needs the results of the three previous time steps [32]. Therefore the first three steps are evaluated using the Runge-Kutta algorithm.

### G. Initial conditions

Inverse *Bremsstrahlung* is the only absorption mechanism taken into account, so that this model is not able to calculate the early stage of the plasma, in which the first free electrons are created by multiphoton ionization (MPI). Also the presence of molecules and of two aggregation stages would make the model much more complicated. Therefore the calculation starts with a fully dissociated plasma in which inverse *Bremsstrahlung* is dominant. The point in time $t_0$ when this occurs depends on two facts: (1) the irradiance of the laser has to exceed a certain threshold $I_{\mathrm{MPI}}$ (around $4.5\times10^{11}\ \mathrm{W\,cm^{-2}}$ at 532 nm [34]) in order to create the first electrons by MPI and (2) a certain amount of absorbed energy $E_0$ is necessary to evaporate and to dissociate the water molecules, and to bring the electron density to a significant value ($>10^{25}\ \mathrm{m^{-3}}$), so that inverse *Bremsstrahlung* incoupling can be effective.

Above the mentioned density inverse *Bremsstrahlung* is the dominant absorption mechanism, see Sec. II D. At the start of the calculation the plasma radius is assumed to be equal to the initial droplet radius (10 $\mu$m) and the initial expansion velocity is assumed to be zero.

The minimum energy per water molecule necessary to bring the plasma in the condition as described above is thus

$$E_0>E_{\mathrm{evap}}+E_{\mathrm{disso}}+E_{\mathrm{ion}}+E_{\mathrm{th}}+E_{\mathrm{exp}}\approx E_{\mathrm{evap}}+E_{\mathrm{disso}}+U_{\mathrm{int},0}\approx 10\ \mathrm{eV}+U_{\mathrm{int},0}. \tag{45}$$

After the MPI threshold has been reached, the model waits until $E_0=1.6\times(E_{\mathrm{evap}}+E_{\mathrm{disso}})\approx16\ \mathrm{eV}$ has been absorbed per molecule, before it starts the real calculations. During this initial phase an absorption of 25% of the laser light hitting the droplet is assumed. The energy exceeding the dissociation and evaporation energy, i.e., ≈6 eV per molecule, is assumed to be in the plasma as initial internal energy $U_{\mathrm{int},0}$, which for the above numbers lead to $T=1.26\ \mathrm{eV}$ and $n_e=1.1\times10^{26}\ \mathrm{m^{-3}}$.

The influence of those initial conditions on the results is discussed in Sec. III B.

## III. RESULTS AND DISCUSSION

The program has been coded in C++ and can be run on any Un*x workstation or on a PC running LINUX or WIND*ws. Care has been taken to write reusable code. The parameters (geometry, laser settings, material, atomic properties) are read from a hierarchically organized input file and parsed by the PLASIMO parser code [35]. For user's convenience, the most important parameters can be overridden by command line options or automatic (one-dimensional) optimization runs can be carried out.

On an Athlon-700 PC running LINUX, a run with the standard parameter set takes about half an hour, calculating ≈460 time steps of 25 ps each. Plasma parameters, radiation, etc. are written to log files for every time step and in the end some integrated values, such as energies (e.g., absorbed laser) are output.

By far the most time (around 99%) is spent in the calculation of the radiation, as a complete spectrum has to be produced every time step, to yield a correct integrated spectrum in the end and to correctly account for the radiative loss term in the energy equation. Some techniques have been applied to speed this up, such as creating a sorted list of the free-bound edges and use interpolation for the values in between. This has been verified not to yield any error exceeding a per mille in the radiation calculations.

### A. Results of the model

The modeled results for the same conditions as in the experiment (see Sec. I) are given in Figs. 2 and 3. It is assumed that the temporal profile of the laser intensity has a parabolic shape with a length of 10-ns FWHM and centered around the time $t=0$ and thus starts at $t_{\mathrm{start}}=-7.07$ ns. After 430 ps the MPI threshold is reached and another 620 ps later the required energy $E_0$ has been absorbed. The $1.4\times10^{14}$ water molecules in the droplet are dissociated by then.

The laser is now coupled into the plasma rather efficiently and the electron density $n_e$ and the plasma temperature $T$ increase at a high rate. The heating leads to a sharp increase in the pressure $p=n_ek_BT$, which in turn causes the expansion $v_{\mathrm{exp}}$ of the plasma to accelerate and thus slowing down the increase in electron density.

Half a nanosecond later ($t\approx-5.45$ ns), the electron density reaches its highest value ($1.27\times10^{28}\ \mathrm{m^{-3}}$). It is now high enough, that half (47%) of the laser power is reflected at the interface between the vacuum and the plasma. The radius of the plasma has 14 $\mu$m, and half of the oxygen atoms are ionized at a plasma temperature of 6.0 eV.

After 1.25 ns (at $t\approx-4.2$ ns), the emission between 7 and 16 nm wavelength (subsequently referred to as EUV emission) reaches it maximum of $P_{\mathrm{EUV,max}}=1.2\ \mathrm{MW}$. The plasma has a temperature of 17.7 eV and the oxygenic ionization ratio

$$\alpha_O=\frac{\Sigma_Z Z n_{\mathrm{O}}(Z)}{\Sigma_Z n_{\mathrm{O}}(Z)} \tag{46}$$

is at 4.84 and is quickly approaching the ideal value of about 5. This value is considered ideal because the line around 13

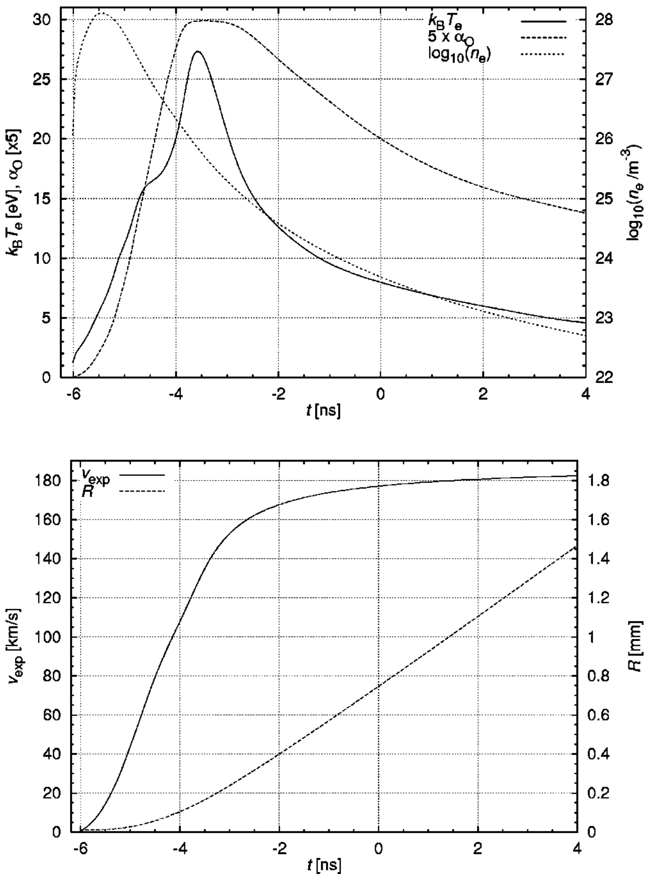

FIG. 2. The time evolution of the plasma quantities as calculated by the model for a 10-$\mu$m-radius water droplet irradiated by a 0.45-J laser pulse with 10-ns FWHM parabolic shape focused to a focal radius of 20 $\mu$m. First picture: electron density $n_e$, plasma temperature *T*, and the ionization ratio $\alpha_O$ of oxygen; second picture: expansion velocity $v_{exp}$ and radius *R* of the droplet.

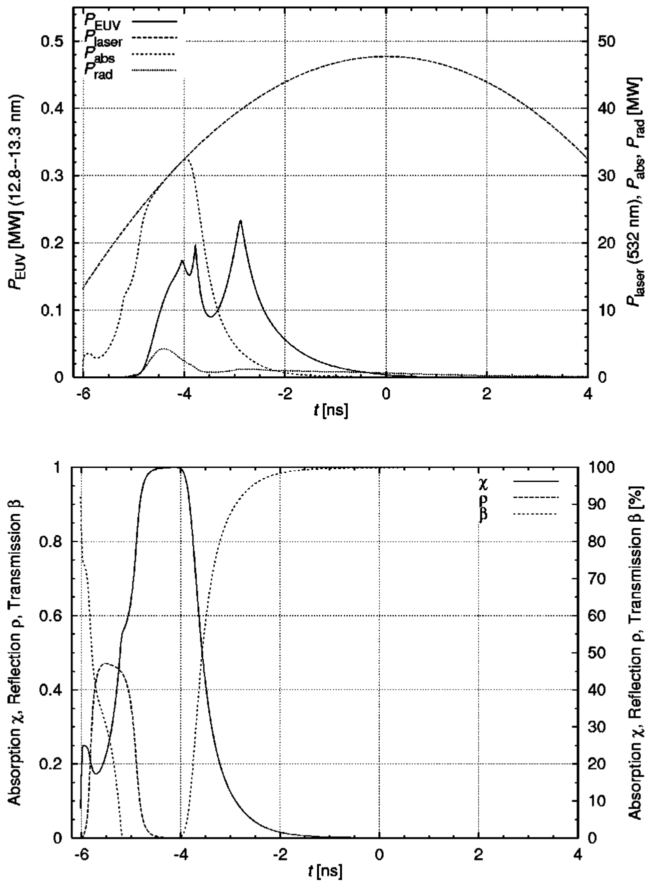

FIG. 3. The time evolution of radiation quantities for the same parameters as above (Fig. 2) as predicted by the model. First picture: EUV (12.8–13.3 nm) yield $P_{EUV}$ total radiation $P_{rad}$ of plasma, laser power input $P_{laser}$, and absorption $P_{abs}$; second picture: coefficients for absorption $\chi$, reflection $\rho$, and transmission $\beta$ of the laser.

nm is produced by the $4d \rightarrow 2p$ transition in $O^{5+}$. The maximum in the radiation from this line occurs a bit later at $t \approx -4.05$ ns and the oxygenic ionization ratio is already at 5.36 then. The higher temperature of 19.3 eV seems to compensate that slight "overheating" and $P_{13\,\mathrm{nm,max}} = 0.17$ MW of 13 nm (12.8–13.3 nm) radiation is produced. The plasma absorbs almost 100% of the laser power at that moment and has expanded by a factor of 10 in radius (factor 1000 in volume). The electron density is only 2% of its maximum value. The plasma radius increases with $v_{exp} = 105$ km/s. About half of the oxygen atoms are five times ionized, which corresponds $7.3 \times 10^{13}$ atoms and a density $n_{O^{5+}} \approx 1.75 \times 10^{25}$ m$^{-3}$ of $O^{5+}$.

The oxygenic ionization ratio $\alpha_O$ continues to increase as does the plasma temperature. The temperature *T* reaches its maximum of 27.3 eV another 475 ps later, followed by the maximum in the oxygenic ionization ratio of 5.98 after 125 more ps. The EUV radiation has dropped to a third of its maximum value. Only a third of the laser power can still be absorbed due to the fallen electron density.

The oxygenic ionization ratio starts to drop and approaches a value of 5 again. This slows down the decrease in EUV output a little bit. However, when it reaches 5 around $t = -1.55$ ns, the temperature with 11.0 eV is much lower than 2.6 ns earlier due to the decreased density that shifts the Saha balance (17) to the right. Thus, far less radiation is produced, as the distribution of excited states inside the ionic systems is just determined by the temperature *T* according to the Boltzmann distribution.

The decrease of the electron density $n_e$ has another effect: The absorption of the laser dropped to almost zero; the plasma is almost transparent for the laser light. The maximum of the laser pulse has not yet been reached, but the laser does not have much interaction with the plasma any more.

The expansion velocity $v_{exp}$ has now almost reached its maximum value of about 183 km s$^{-1}$ (corresponding to a kinetic energy of 2.8 keV for oxygen atoms). It is still increasing very slowly due to the conversion of internal energy (excitation, ionization) into kinetic energy. It should be noted that the plasma is not well described by the model any longer, as due to the fallen density, the equilibrium relations do not hold any longer. This will be discussed in the following section.

It is remarkable that only are small part of the laser energy ($E_{laser} = 450$ mJ) gets absorbed by the plasma: $E_{abs} = 53.9$ mJ, which corresponds to 12.0%. A small fraction is

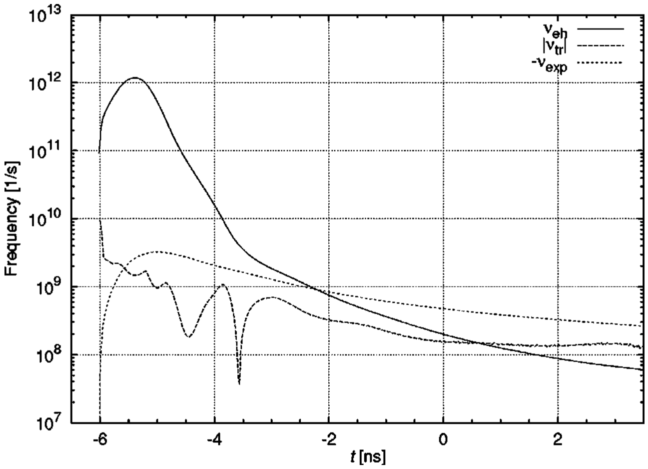

FIG. 4. Frequencies related to the thermal equilibrium as a function of time $t$ using the results of the calculation. The equilibrium restoring frequency $\nu_{eh}$ is larger than the disturbing frequencies for $t < -2.5$ ns.

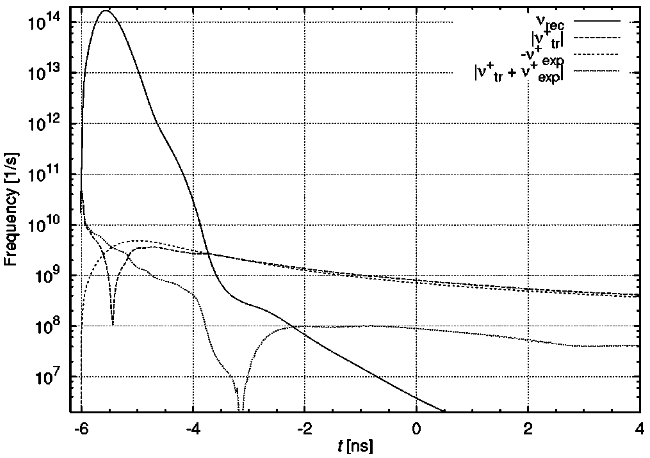

FIG. 5. Frequencies related to the Saha equilibrium as a function of time using the results of the model. Note that the effects of the expansion and the transient partially cancel each other, which can be seen by looking at $|\nu^+_{\rm tr} + \nu^+_{\rm exp}|$. This is fortunate as the Saha equilibrium can be maintained till $t = -2.5$ s.

reflected (1.9%) and the largest fraction (86%) is transmitted.

When the model stops running, about 3 mJ are still in thermal and internal energy. However, the largest part of the absorbed energy went into the expansion: 42.3 mJ corresponding to 78.5%. Only 12.5 mJ (15.0% of the absorbed energy) went into radiation and only a small part of it is in the interesting wavelength region 12.8–13.3 nm: 0.39 mJ.

This yields an overall conversion efficiency (CE) of laser energy into 13-nm EUV output of 0.9‰. The spectrum of the emission is also output by the model and presented in Fig. 6 in comparison to experimental data.

Line radiation accounts for 82% of the total emission (all wavelengths), 17% comes from recombination radiation, and the rest (1.2%) is from *Bremsstrahlung*.

### B. Validity of thermal equilibrium and sensitivity to parameter changes

In Sec. II C the question whether transient effects would significantly disturb the plasma's thermodynamic equilibrium could not be answered, as the rates of equilibrium restoring processes have to be compared to the change rates of plasma parameters. This check can be performed now with the results.

Figures 4 and 5 show a comparison of the frequencies related to the equilibrium conditions. The equilibrium approximations are valid for $t < -2.5$ ns. This limitation is less serious than it sounds: All the interesting processes, such as absorption of the laser and emission of EUV happen before this, so the model should give reasonable predictions nevertheless. The maximum expansion velocity is almost reached by that time, so this result of the model should not be strongly affected either.

According to the model results, after $t = -2.5$ ns, the recombination rate is too low to preserve the Saha equilibrium; this will most likely lead to an overpopulation of higher ionization states compared to the equilibrium situation. The cooling by expansion lowers the kinetic (thermal) energy of the heavy particles and free electrons.

The atomic state distribution function will be affected by the too low electron-ion collision frequency $\nu_{eh}$. Highly excited states will stay a bit longer in partial Saha equilibrium, i.e., be in Saha equilibrium with the ground state of next ionization stage; less highly excited states, however, will be largely affected by radiative transitions. This might lead to conditions where overpopulation of some states with respect to lower states can be found, the conditions needed for lasing.

Normally time steps of 25 ps are being used in the model. This choice has been determined by running the model with different time steps; significantly larger time steps do show slightly different results, indicating loss of accuracy due to too large time steps. Smaller time steps, on the other hand, did not show any changes.

The dependence of the results on other input parameters and initial conditions have been investigated in order to test for the sensitivity on the (slightly arbitrary) choice of initial conditions on one hand, and to see the results of changed experimental parameters on the other.

The focal radius of the laser does hardly change the results. Doubling the focal radius from 10 to 20 $\mu$m leads to a slightly hotter plasma (35 eV), whereas the total EUV output increases by just 2%. The weak dependence of the focal radius is not surprising, taken that the droplet radius very quickly expands to exceed the size of the laser focus.

The initial conditions $v_{\rm exp,0}$, $U_{\rm int,0}$ do not have any significant influence on the results. Taking the initial expansion velocity to be equal to the ion acoustic velocity, e.g., does lead to identical results, as the expansion due to the heat generated pressure is much larger anyway. However, when choosing $E_0$ [cf. Eq. (45)], it needs to be chosen large enough to produce a not too small electron density, so that the equilibrium assumptions hold. Varying it from 15 eV to 20 eV also did not show any noticeable changes in the results. This is to be expected, as the most important quantity in physics, the energy, is being preserved, regardless. The

MPI threshold may not be varied too much; with the long laser pulse of the experimental conditions investigated here, with consequently bad absorption as the expansion is too quickly lowering the density, a higher threshold resulting in a later start of the model leads to more absorbed power and thus a hotter plasma.

Changing the laser pulse shape from parabolic to Gaussian (keeping the same FWHM and energy) leads to a slight decrease in conversion efficiency. For a FWHM = 10-ns Gaussian laser pulse, the plasma gets less hot (26.2 eV instead of 27.4 eV), 3.5% less laser power is absorbed and the conversion efficiency raises a tiny bit from 0.896‰ to 0.900‰.

The changing the energy of the laser pulse shows some significant influence. The maximum plasma temperature shows some more or less linear dependence on the laser energy. For lower energies, the less strong overheating leads to a better conversion efficiency, but the absolute EUV output drops. When going to rather high energies, the self-stabilizing effect of reflection, if $n_e$ gets too high (see Sec. II D), limits the heating.

The most sensitive parameters are the initial droplet size and laser pulse length (FWHM). Using larger droplets leads to colder plasmas, of course. If the laser energy is corrected for this, one can see, that the larger mass (inertia) of the droplet leads to a bit slower expansion. The electron density thus drops less fast and more power is being coupled in. Consequently, a larger fraction of the energy goes into emission instead of expansion. Using shorter pulses also leads to a strong increase in EUV output, as more of the laser energy is coupled in when the plasma still has a high electron density and thus high absorption. For example 2 using a 8-ns FWHM parabolic laser pulse of 450 mJ leads to higher fraction of the laser energy being coupled in (14% instead of 12%), a maximum temperature of 37 eV instead of 28 eV, but only yields about the same amount of EUV as the overheating gets worse. If compensated with larger droplets, or lower laser energies, significantly better conversion efficiencies can be reached, see Sec. III D.

### C. Comparison with measurements

Only few time-resolved data could be found for laser-produced water droplet sources. Constantinescu *et al.* [7,15] measured the EUV output for different angles as a function of time. (Take care when comparing Fig. 9 of that article to Fig. 3 of this article: The laser has been offset to the left there.) The EUV emission is reported to be close to isotropic there and the duration of the emission (FWHM≈5 ns) is much shorter than the laser pulse, which is also predicted by the model. The temporal behavior also is slightly asymmetric with a rise time being shorter than the fall time. However, the EUV pulse length is significantly larger than the modeled one (FWHM≈2 ns). This may be explained by the fact, that the EUV diodes used in the measurement are sensitive from 7–17 nm and an average over 10 shots was taken, thus allowing small variations to broaden the time profiles. Accounting for 7–17 nm in the model results in a EUV pulse length (FWHM) of ≈3.5 ns. Given that the measurements are averaged over several pulses, a small jitter may be the reason for the slightly longer EUV pulse length observed.

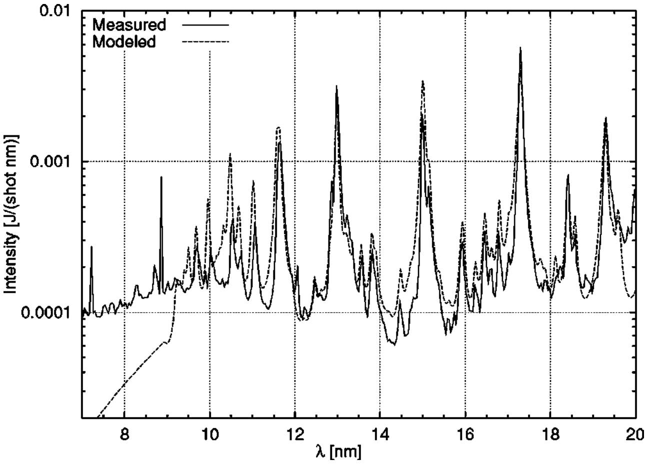

FIG. 6. Spectrum as measured in comparison with the modeled spectrum. The distribution of the intensities of the modeled spectrum matches the measured distribution quite well. For comparison the lines of the calculated spectrum are broadened with the apparatus profile of the spectrometer. Below 9 nm, which corresponds to 138 eV, the ionization energy from $O^{5+}$ to $O^{6+}$, the free-bound emission can be recognized in both the model and the measurement. The measured spectrum has been scaled to match the intensity reported by Ref. [15]. The measured spectrum has been corrected for the transmission of the zirconium filter, Ref. [36].

The measured isotropic distribution of the emission is in agreement with the assumption of homogeneity (Sec. II A) more exactly it implies spherical symmetry or an optically open plasma.

In Fig. 6 the calculated, time-integrated spectrum is compared to the measured one (see Ref. [15]). The quantitative agreement is rather good. In the calculation a total EUV flux at 13 nm of $2.01\times10^{12}$ photons/shot sr is found, which matches the measured intensity [15] up to a few percent. It should be noted that the measured intensity has a high uncertainty, due to uncertainties with respect to the transmission of the grating used.

When comparing the shape of the spectrum, one can see that the line spectrum matches rather well. For the positions of the lines, this is not giving much information about the accuracy of the model, as these are defined by the atomic data used. The relative intensities, however, give an indication whether the temperature as calculated in the model and the distribution of states as a consequence of the equilibrium assumptions are valid. The agreement is reasonable. The line widths visible in this figure stem from the spectrometer profile mainly; the line broadening is weaker.

However, the region below 9 nm, where the recombination (free-bound) radiation dominates, the experiment yields clearly more radiation. The absolute magnitude of the recombination radiation is not easy to get very exact, because one needs to sum over many levels and always has Gaunt factors that may not be very exact, as they have been calculated for hydrogen originally.

More important, the slope of the free-bound feature is different, which is an indication of too low temperature in

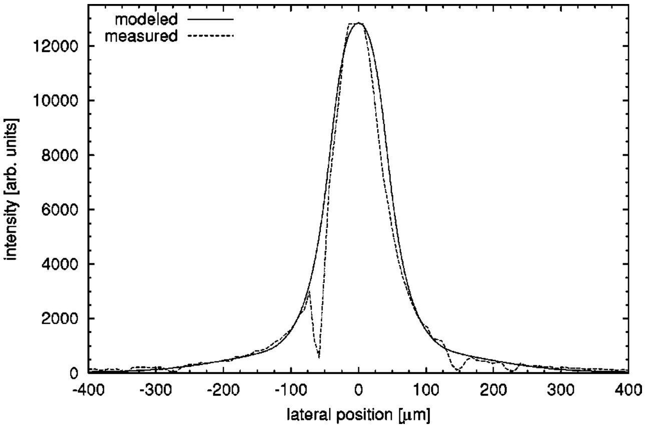

FIG. 7. The shape of the modeled EUV (7–16 nm) intensity distribution as a function of lateral position resembles the measured one quite well. The rough structure in the measured distribution is due to the support structure of the Zr filter that is used to block the visible light and placed in between the plasma and the pinhole camera. Both measured and calculated intensities are line-of-sight integrated values. No Abel inversion has been performed. The model data have been scaled to match the measurement as no calibration for absolute intensities had been performed in the measurement.

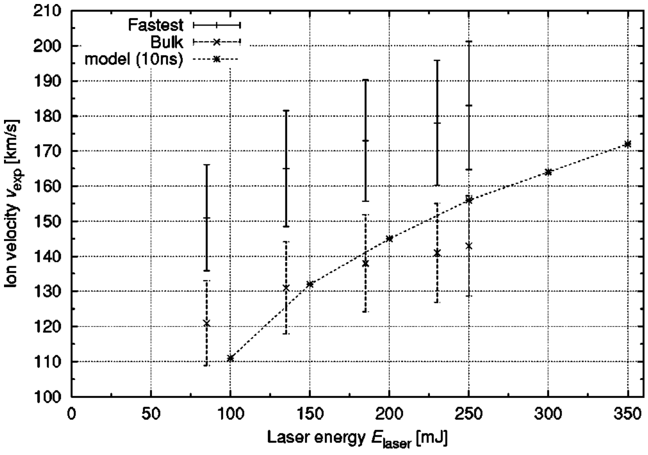

FIG. 8. Ion velocity vs laser pulse energy. The time between the start of the laser pulse and the arrival of the first (denoted as "Fastest") and the main part ("Bulk") has been measured. Errors are due to the uncertainty in the exact distance between detector and source. Parameters used: 10-ns parabolic 532-nm laser pulse, focused on 10-μm water droplets with 20-μm focal radius.

the model, as the slope mainly depends on the temperature (and weakly on the Gaunt factors). This part of the spectrum matches rather well—both slope and magnitude—with a plasma that is considerably hotter, around 65 eV. As the maximum temperature is very sensitive to the pulse length, this could be an explanation. However, one needs to use pulse lengths below 4 ns to get to such high temperatures in the model, so this does not explain the discrepancy.

A more likely explanation is that the assumption of homogenous temperature distribution of the plasma is too crude. While the line spectrum is not so much affected by this, the recombination radiation is rather sensitive to the temperature. A hot spot can emit a large amount of recombination radiation, while the cooler part is the main contributor to the line spectrum.

The first picture of Fig. 3 shows that according to the model most of the EUV intensity is emitted in a relatively short interval between $t=-4.5$ ns and $t=-2.5$ ns. The calculated plasma radius varies between 60 μm and 300 μm in this time, which can be compared to the measured plasma size of 135 μm. (See Fig. 7.)

Pinhole pictures (Fig. 7) of the plasma have been taken with photodiodes, which were protected by a zirconium filter, yielding a time-integrated image of the emission between 7 and 16 nm. The size of the imaged emission can be related to the size of the plasma when EUV radiation is strongest and thus gives information about the relation between the time the plasma needs to build up and the time it takes to expand. The model predicts this very well.

Ion speed measurements have been carried out by measuring the time difference between the start of the laser pulse and the detection of ions by a probe located at a certain distance from the plasma similar as in e.g., Refs. [37,38]. Figure 8 shows the results of those measurements for different laser energies in comparison with the modeled results. The modeled results should—expect for fluctuations that exist in reality but not in the model—be close to the speed of the fastest ions, and certainly be above the bulk of ions. However, the modeled speed is closer to the measured bulk speed than to the measured top speed. Also here, the simplification of using a homogeneous sphere may be responsible: We neglect variations in the temperature that would cause a spread in velocities. It should also be noted that the velocities as result of the model depend rather sensitively on the laser pulse length, which was not very exactly determined in this experiment. Still, overall agreement on ion speeds can be considered satisfactory in the scope of this comparably simple model.

### D. Optimization of the plasma

The results show that only 12% of the laser pulse is absorbed. This is due to the low density after some expansion has been taken place, which means that the second half of the laser pulse is just wasted. Furthermore, from this absorbed energy, the main fraction (>75%) goes into expansion, only the rest can be radiated. And only a part of this can be found in the interesting spectral range. Overall conversion efficiency (defined here as total emitted EUV between 12.8 and 13.3 nm divided by laser energy) is only 0.09%.

Optimization strives to increase this efficiency (or the absolute output). Furthermore, the high kinetic energy of 2.8 keV of the oxygen ions from the expanding plasma does pose a serious debris problem [7], as those ions are likely to sputter the mirrors. Reducing the energy that goes into the expansion will help here and fortunately does not contradict with increasing the energy that is radiated.

From these observations, it becomes clear how to optimize the plasma. First, the pulse needs to be shorter or the expansion needs to be slowed down by, e.g., increasing the mass of the droplets in order to couple more energy into the plasma. It should be avoided to overheat the plasma too strongly, i.e., ionize a significant amount of oxygen more than five times.

The moderate run time of the model allows to check with a variety of parameters. A number of calculations have been performed to find optimal parameters. Good results have been found for water droplets of 19 $\mu$m radius, irradiated by a 4-ns FWHM 0.45-J laser pulse (where more than 75% of the laser power is absorbed), a CE of 0.66% can be reached, and the energy of the emerging oxygen ions is slightly decreased to 2.5 keV.

Experiments carried out at Philips Research Laboratories in Eindhoven have confirmed that larger droplets lead to an increase in conversion efficiency. Shorter laser pulses could unfortunately not be tested.

However, shorter pulses are also predicted to yield better efficiency by Jin and co-workers [39], Fig. 5(c). The x-ray output does stay constant at decreasing pulse length with constant laser intensity, i.e., decreasing laser energy, which means that the conversion efficiency improves.

The model has also been used to do numerical experiments with prepulses; however, in the investigated parameter range, applying a prepulse leads to worse results. Considering that the fast expansion process does limit the laser energy coupled in, it is not surprising that starting the expansion earlier does not improve the situation. If much shorter pulses were to be used, prepulses might achieve improvements.

The total amount of radiation that comes out of the water droplet plasma probably can still be increased somewhat. It is still far below the Planck limit, so this will not limit tries to improve EUV output. On the other hand, oxygen molecules are rather light elements and are easily accelerated, therefore a large fraction of energy will always be found in kinetic energy. And the part that is radiated is spread over a range of wavelengths depending on the electronic structure of the ions involved.

## IV. CONCLUSIONS AND OUTLOOK

In conclusion, we can state that the special conditions in these mass-limited targets allow for a significant simplification of the model. The resulting relatively simple model gives a reasonable agreement with the present experimental results.

The assumption of a homogeneous sphere in the model is the most critical one; it incurs a much simpler description of the plasma, but is probably also responsible for some of the deviations found when comparing to the experimental results; the recombination radiation features in the spectrum expose the fact that higher temperatures are present in the plasma. The overall conversion efficiency and overall energy balance (as can be estimated from kinetic energy of the ions) on the other hand do not seem to be affected very strongly, so the model can be used to study the physics of the plasma and predict trends concerning the influence of different parameters on conversion efficiency and ion speeds.

The model exposes the fact that only the first part of the laser pulse is absorbed well as the expansion takes place too fast. The model predicts that by using shorter laser pulses and larger droplets an increase in conversion efficiency to EUV can be achieved. For the droplet size, this has been confirmed by own experiments, whereas results confirming the increased efficiency could be found in literature [39].

However, the conversion efficiency of laser energy into the wanted radiation around 13 nm is still poor; the investigation of other (mass-limited) targets for laser-produced plasmas will be done in the future. It is expected that the model presented here can be adapted to and subsequently applied to those plasmas as well. For lower densities a non-equilibrium model will be needed. The work should be applicable to plasmas with similar temperatures and densities as well and some investigations on plasma channels for laser plasma wakefield acceleration [40–42] are being looked into.

The calculation of the radiation has been paid special attention to as it constitutes the application of the plasma as EUV source; more work on this is planned and will be submitted for publication in a subsequent article.

## ACKNOWLEDGMENTS

The work of the authors has been carried out at Philips Research Laboratories (''Nat.Lab.''), Eindhoven, NL, where the water droplet source has been operated, and the measurements and the initial work on modeling have been done. The work was part of a project on the investigation of possible light sources for future lithography technologies, supported and financed by ASML, Veldhoven, NL. Thanks are specifically due to Vadim Banine (ASML) for his support with respect to discussions about the requirements and possible setup for such a light source and his support for the project. From the University side, the project is supported by the CPS (Center for Plasma Physics and Radiation Technology). The authors would like to thank their colleagues for helpful discussions. Thanks go especially to Professor D. C. Schram for always having useful and critical but also supportive comments.

---

[1] C. Gwyn, R. Stulen, D. Sweeney, and D. Attwood, J. Vac. Sci. Technol. B **16**, 3142 (1998).

[2] I. Turcu and J. Dance, *X-Rays from Laser Plasmas: Generation and Application* (Wiley, West Sussex, 1999).

[3] G. Stix, Sci. Am. **284**(4), 20 (2001); http://www.sciam.com/2001/0401is-sue/0401innovations.html

[4] J. Kirz, C. Jacobsen, and M. Howells, Q. Rev. Biophys. **28**, 33 (1995).

[5] D. Colombant and G. Tonon, J. Appl. Phys. **44**, 3524 (1973).

[6] M. Richardson, D. Torres, C. DePriest, F. Jin, and G. Shimkaveg, Opt. Commun. **145**, 109 (1998).

[7] R. Constantinescu, J. Jonkers, and J. Vrakking, in *Proceedings*

*of the Technical Digest OSA Conference: Applications of High Field and Short Wavelength Sources VIII, Potsdam, Germany, 1999* (Optical Society of America, Washington, DC, 1999), p. 111.

[8] G. Kubiak, L. Bernardez, K. Krenz, D. O'Connell, R. Gutowski, and A. Todd, *Extreme Ultraviolet Lithography*, Trends in Optics and Photonics Vol. 4, edited by D. Kania (Optical Society of America, Washington, DC, 1996).

[9] L. Rymell and H. Hertz, Opt. Commun. **103**, 105 (1993).

[10] H. Hertz, L. Rymell, M. Berglund, and L. Malmqvist, Proc. SPIE **2523**, 88 (1995).

[11] L. Rymell, M. Berglund, and H. Herz, Appl. Phys. Lett. **66**, 2625 (1995).

[12] M. Berglund, L. Rymell, and H. Hertz, Appl. Phys. Lett. **69**, 1683 (1996).

[13] C. Gwyn *et al.*, *Extreme Ultraviolet Lithography, a White Paper* (EUV LLC, Livermore, CA, 1998).

[14] G. Schriever, K. Bergmann, and R. Lebert, J. Vac. Sci. Technol. B **17**, 2058 (1999).

[15] R. Constantinescu, J. Jonkers, P. Hegemann, and M. Visser, Proc. SPIE **4146**, 101 (2000).

[16] M. Richardson, D. Torres, C. DePriest, F. Jin, and G. Shimkaveg, Proc. SPIE **3157**, 306 (1997).

[17] M. Visser, R. Constantinescu, P. Hegeman, J. Jonkers, M. Dekker, E. Louis, and D. Hambach, Proc. SPIE **3997**, 733 (2000).

[18] J. v. d. Mullen and J. Jonkers, Spectrochim. Acta, Part B **54**, 1017 (1999).

[19] M. Mitchner and C. Kruger, *Partially Ionized Gases* (Wiley, New York, 1977).

[20] M. Boulos, P. Fauchais, and E. Pfender, *Thermal Plasmas: Fundamentals and Applications* (Plenum, New York, 1994).

[21] J. v. d. Mullen, Ph.D. thesis, Technische Universiteit Eindhoven, Faculteit Natuurkunde, ETP, 1986 (unpublished).

[22] T. Hughes, *Plasmas and Laser Light* (Adam Hilger, Bristol, 1975).

[23] T. Johnston and J. Dawson, Phys. Fluids **16**, 722 (1973).

[24] E. Hecht, *Optics*, 3rd ed. (Addison-Wesley/Longman, London/New York, 1998).

[25] P. Brussaard and H. van de Hulst, Rev. Mod. Phys. **34**, 507 (1962).

[26] D. Menzel and C. Pekeris, Mon. Not. R. Astron. Soc. **96**, 77 (1935).

[27] Amods Atomic Spectral Line Database (2001), http://amods.kaeri.re.kr/spect/SPECT.html

[28] P. Smith, J. E. C. Heise, and R. Kurucz, Atomic Spectral Line Database (2001), http://www.pmp.uni-hannover.de/projekte/kurucz/sekur.html

[29] D. Salzmann, *Atomic Physics in Hot Plasmas* (Oxford University Press, New York, 1998).

[30] H. Griem, *Spectral Line Broadening by Plasmas* (Academic, New York, 1974).

[31] W. Martin and W. Wiese, in *Atomic, Molecular and Optical Physics Handbook*, edited by G. Drake (AIP Press, Woodbury, NY, 1996); http://physics.nist.gov/Pubs/AtSpec/

[32] E. Kreyszig, *Advanced Engineering Mathematics*, 7th ed. (Wiley, New York, 1993).

[33] W. Press, S. Teukolsky, W. Vetterling, and B. Flannery, *Numerical Recipes in C*, 2nd ed. (Cambridge University Press, Cambridge, 1992).

[34] A. Vogel, K. Nahen, D. Theisen, and J. Noack, IEEE J. Sel. Top. Quantum Electron. **2**, 847 (1996).

[35] J. van Dijk, Ph.D. thesis, Technische Universiteit Eindhoven, Faculteit Natuurkunde, ETP, 2001.

[36] Berkeley Lab, Center for X-ray Optics, Atomic scattering factors (2001), http://www-cxro.lbl.gov/optical_constants/

[37] R. von Gutfeld and R. Dreyfus, Appl. Phys. Lett. **54**, 1212 (1989).

[38] P. Dyer, R. Greenough, A. Issa, and P. Key, Appl. Phys. Lett. **53**, 534 (1988).

[39] F. Jin and M. Richardson, Appl. Opt. **34**, 5750 (1995).

[40] E. Esarey, P. Sprangle, J. Krall, and A. Ting, IEEE Trans. Plasma Sci. **24**, 252 (1996).

[41] D. Spence, A. Butler, and S. Hooker, J. Phys. B **34**, 4103 (2001).

[42] N. Bobrova, A. Esaulov, J.-I. Sakari, P. Sasorov, D. Spence, A. Butler, S. Hooker, and S. Bulanov, Phys. Rev. E **65**, 016407 (2002).